

damping. None of the above processes in early lunar evolution are well explored.

References and Notes

1. P.-S. Laplace, *Traité de Mécanique Céleste* (Paris Duprat, Bachelier 1798-1827), vol. 2, book 5, chap. 2.
2. W. F. Sedgwick, *Messenger Math.* **27**, 171 (1898).
3. H. Jeffreys, *Mem. R. Astron. Soc.* **60**, 187 (1915).
4. H. Jeffreys, *Mon. Not. R. Astron. Soc. Geophys. Suppl.* **4**, 1 (1937).
5. H. Jeffreys, *The Earth* (Cambridge Univ. Press, Cambridge, 1970).
6. A. S. Konopliv et al., *Science* **281**, 1476 (1998).
7. J. G. Williams, D. H. Boggs, C. F. Yoder, J. T. Ratcliff, J. O. Dickey, *J. Geophys. Res.* **106**, 27933 (2001).
8. Z. Kopal, *Proc. R. Soc. London Ser. A* **296**, 254 (1967).
9. P. Goldreich, A. Toomre, *J. Geophys. Res.* **74**, 2555 (1969).
10. M. Lefftz, H. Legros, *Phys. Earth Planet. Inter.* **76**, 317 (1993).
11. K. Lambeck, S. Pullan, *Phys. Earth Planet. Inter.* **22**, 29 (1980).
12. S. K. Runcorn, *Nature* **195**, 1150 (1962).
13. P. Cassen, R. E. Young, G. Schubert, *Geophys. Res. Lett.* **5**, 294 (1978).
14. D. J. Stevenson, *Proc. Lunar Planet. Sci. Conf. XXXII*, abstract 1175 (2001).

15. S. Zhong, M. T. Zuber, *J. Geophys. Res.* **105**, 4153 (2000).
16. G. A. Neumann, M. T. Zuber, D. E. Smith, F. G. Lemoine, *J. Geophys. Res.* **101**, 16841 (1996).
17. T. Kleine, H. Palme, K. Mezger, A. N. Halliday, *Science* **310**, 1671 (2005).
18. C. D. Murray, S. F. Dermott, *Solar System Dynamics* (Cambridge Univ. Press, Cambridge, 1999).
19. J. Touma, J. Wisdom, *Astron. J.* **108**, 1943 (1994).
20. R. D. Ray, R. J. Eanes, F. G. Lemoine, *Geophys. J. Int.* **144**, 471 (2001).
21. The Hansen functions, $X_{l,p,q}(e)$, satisfy $(\frac{d}{dt})^l \cos(pf) = \sum_q X_{l,p,q}(e) \cos(q\tilde{M})$ (32), where f is the true anomaly and \tilde{M} is the mean anomaly. For our purposes, $l = -3$. The Hansen functions are also called Hansen coefficients, and the expansions in e to fourth order can be found in table 3.2 of (33), albeit with a different subscript convention.
22. S. J. Peale, P. Cassen, *Icarus* **36**, 245 (1978).
23. C. F. Yoder, in *Global Earth Physics*, T. J. Ahrens, Ed. (American Geophysical Union, Washington, DC, 1995), p. 1.
24. The simple average of two different sets of parameters β , γ , and C_{20} may take place during the transition from the state of low relaxation time to the state of long relaxation time. During this time, the Moon is plastic enough to accommodate changes in form, yet stiff enough to retain some signature of its state when freeze-in started. Indeed, the

Moon is necessarily a sum of different orbits, however close or far apart, if the fossil bulge hypothesis is valid.

25. P. Goldreich, *Mon. Not. R. Astron. Soc.* **126**, 257 (1963).
26. S. J. Peale, *Celest. Mech. Dyn. Astron.* **87**, 129 (2003).
27. J. Touma, J. Wisdom, *Astron. J.* **115**, 1653 (1998).
28. E. Kokubo, S. Ida, J. Makino, *Icarus* **148**, 419 (2000).
29. P. Goldreich, S. J. Peale, *Astron. J.* **71**, 425 (1966).
30. S. J. Peale, in *Satellites*, J. A. Burns, Ed. (Univ. of Arizona Press, Tucson, 1978), p. 87.
31. Mercury's unnormalized coefficients $C_{20} = 6 \times 10^{-5} \pm 2.0$ and $C_{22} = 1 \times 10^{-5} \pm 0.5$ (34) are not reproduced by any orbit-spin resonance at Mercury's current semimajor axis.
32. H. C. Plummer, *An Introductory Treatise on Dynamical Astronomy* (Dover, New York, 1960).
33. W. M. Kaula, *Theory of Satellite Geodesy* (Dover, New York, 1966).
34. J. D. Anderson, G. Colombo, P. B. Esposito, E. L. Lau, G. B. Trager, *Icarus* **71**, 337 (1987).
35. We are grateful to B. Hager and B. Weiss for helpful comments. This work was supported by NASA Planetary Geology and Geophysics Program grants (to M.T.Z. and J.W.).

3 April 2006; accepted 8 June 2006
10.1126/science.1128237

Smoke and Pollution Aerosol Effect on Cloud Cover

Yoram J. Kaufman¹ and Ilan Koren^{2*}

Pollution and smoke aerosols can increase or decrease the cloud cover. This duality in the effects of aerosols forms one of the largest uncertainties in climate research. Using solar measurements from Aerosol Robotic Network sites around the globe, we show an increase in cloud cover with an increase in the aerosol column concentration and an inverse dependence on the aerosol absorption of sunlight. The emerging rule appears to be independent of geographical location or aerosol type, thus increasing our confidence in the understanding of these aerosol effects on the clouds and climate. Preliminary estimates suggest an increase of 5% in cloud cover.

Aerosol particles originating from urban and industrial pollution or smoke from fires have been shown to affect cloud microphysics, cloud reflection of sunlight to space, and the onset of precipitation (1, 2). Delays in the onset of precipitation can increase the cloud lifetime and thereby increase cloud cover (3, 4). Research on the aerosol effect on clouds and precipitation has been conducted for half a century (5). Although we well understand the aerosol effect on cloud droplet size and reflectance, its impacts on cloud dynamics and regional circulation are highly uncertain (3, 5–9) because of limited observational information and complex processes that are hard to simulate in atmospheric models (10, 11). Indeed, global model estimates of the radiative forcing due to the aerosol effect on clouds range from 0 to -5 W/m^2 . The reduction of this uncertainty is a major challenge in improving climate models.

Satellite measurements show strong systematic correlations among aerosol loading, cloud cover (12), and cloud height over the Atlantic Ocean (13) and Europe (14), making the model estimates of aerosol forcing even more uncertain. However, heavy smoke over the Amazon forest (15) and pollution over China (16) decrease the cloud cover by heating the atmosphere and cooling the surface (17) and may balance some of this large negative forcing. Global climate models also show a reduction in cloud cover due to aerosol absorption (τ_{abs}) outside (18) and inside the clouds (19). In addition, the aerosol effect on slowing down the hydrological cycle by cooling parts of the oceans (1) may further reduce cloud formation and the aerosol forcing. Understanding these aerosol effects on clouds and climate requires concentrated efforts of measurement and modeling of the effects.

There are several complications to devising a strategy to measure the aerosol effect on clouds. Although clouds are strongly affected by varying concentrations of aerosol particles, they are driven by atmospheric moisture and stability. Local variations in atmospheric moisture can affect both cloud formation and aerosol humidification, resulting in apparent correlations between aerosol column concentration and cloud cover (12, 13, 20).

In addition, chemical processing of sulfates in clouds can affect the aerosol mass concentration for aerosol dominated by sulfates.

We attempt to address these issues by introducing an additional measurement dimension. We stratified the measurements of the aerosol effect on cloud cover as a function of τ_{abs} of sunlight, thus merging in one experiment both the aerosol enhancement and inhibition of cloud cover. Because the concentration of the absorbing component of aerosols is a function of the aerosol chemical composition, rather than aerosol humidification in the vicinity of clouds, this concentration can serve as a signature for the aerosol effect on clouds. A robust correlation of cloud cover with aerosol column concentration and τ_{abs} in different locations around the world can strengthen the quantification of the aerosol effect on cloud cover, though a direct cause-and-effect relationship will await detailed model simulations.

Table 1. Slopes and intercepts of $\Delta f_{\text{ci}}/\Delta \ln \tau$ versus τ_{abs} (Fig. 3A) for the complete data set (All data), continental data dominated by air pollution aerosol, coastal stations, and stations dominated by biomass burning. Results are given for (i) absolute change of the independent cloud fraction Δf_{ci} versus the optical depth $\Delta f_{\text{ci}}/\Delta \ln \tau$ and for (ii) partial change $\delta f_{\text{ci}}/\delta \ln \tau$ from a multiple regression of Δf_{ci} with $\ln \tau$ and total precipitable water vapor.

	Slope versus τ_{abs}		Intercept for $\tau_{\text{abs}} = 0$	
	$\Delta f_{\text{ci}}/\Delta \ln \tau$			
All data	-3.5	-2.6	0.17	0.13
Continental	-3.2	-2.6	0.16	0.13
Coastal	-3.4	-1.9	0.17	0.11
Biomass burning	-4.0	-3.5	0.18	0.14

¹NASA/Goddard Space Flight Center, 613.2, Greenbelt, MD 20771, USA. ²Department of Environmental Sciences and Energy Research, Weizmann Institute, Rehovot 76100, Israel.

*To whom correspondence should be addressed. E-mail: ilan.koren@weizmann.ac.il

The satellite analysis (12–16) may be affected by potential cloud artifacts (21). Therefore, instead of satellite data, we use measurements obtained by Aerosol Robotic Network (AERONET) sunphotometers (22, 23) in 17 sites with long data records and representing different aerosol and climatic regimes (Fig. 1). AERONET measures the aerosol attenuation of sunlight in cloud-free conditions. Although the sunphotometer was not designed to measure cloud cover, clouds affect the interval between consecutive aerosol measurements. We distinguished aerosols from clouds by using spectral variability of three consecutive measurements within 1 min (24). The interval is usually 15 min, but it is too variable to derive the actual cloud cover; however, we can use a systematic variation in the intervals with the aerosol optical thickness τ to derive the change in the cloud cover.

To develop the relationship between the cloud cover and the interval of measurements, let N_0 be the instrumental average rate of measurements per unit of time in the absence of clouds and N be the rate of measurements for a given cloud fraction f_c so that

$$N = N_0(1 - f_c) \quad (1)$$

where f_c is the fraction of the time in which the sunphotometer will detect the cloud and not report aerosol data. The intervals in the sunphotometer measurements are correspondingly $T = 1/N$ and $T_0 = 1/N_0$, where T is the interval between measurements for f_c and T_0 is the interval between measurements for a cloud-free sky. Therefore

$$f_c = 1 - \frac{T_0}{T} \quad (2)$$

Differentiating with respect to the logarithm of τ , a measure of the aerosol column concentration, gives

$$\frac{df_c}{d\ln\tau} = \frac{T_0}{T^2} \frac{dT}{d\ln\tau} \quad \text{or, using Eq. 2:}$$

$$\frac{df_c}{d\ln\tau} = \frac{1}{T} (1 - f_c) \frac{dT}{d\ln\tau} \quad (3)$$

where $df_c/d\ln\tau$ and $dT/d\ln\tau$ are the derivatives of f_c and T , with respect to the logarithm of τ . As the cloud field expands because of an increase in the size or lifetime of the cloud, an overlap among the clouds will mask part of the aerosol effect proportionally to the cloud fraction. This distorts the aerosol effect, particularly for high cloud cover. Therefore, we defined the independent cloud cover change df_{ci} as

$$df_{ci} = \frac{df_c}{(1 - f_c)} = \frac{dT}{T} \quad (4)$$

and used it instead of df_c in this paper. We also tested the AERONET-derived cloud cover against total sky pyranometer measurements (fig. S1).

Figure 2 shows three scatterplots of the interval between adjacent AERONET measurements as a function of τ for different values of τ_{abs} . For each site, 3 to 5 years' worth of data

are separated for every 2 calendar months. We also used the AERONET measurements of τ_{abs} (25, 26). τ_{abs} is accurate within ± 0.01 for a single calibration data set and within ± 0.003 for 5 years of data with approximately six independent calibrations (25, 26). We used τ_{abs} rather than a single scattering albedo because τ_{abs} has very small sensitivity to possible cloud contam-

ination and aerosol humidification. Subvisible clouds, although affecting the scattering in the atmosphere, have almost no effect on absorption and therefore have little influence on τ_{abs} . As the aerosol concentration increases, both the scattering and absorption increase, competing for their effects on the cloud cover. We provide the average values of τ_{abs} for each data set (Figs. 2 and 3),

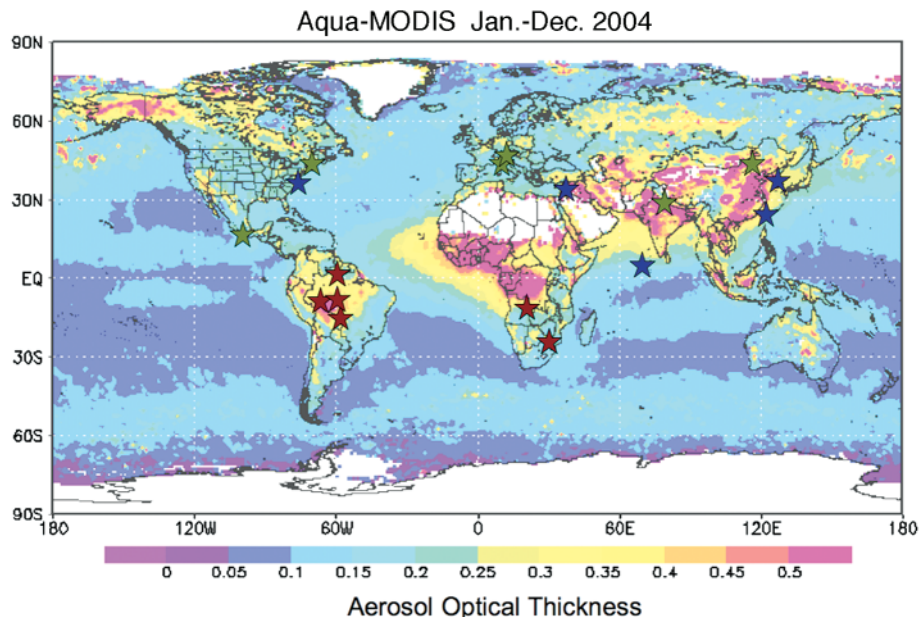
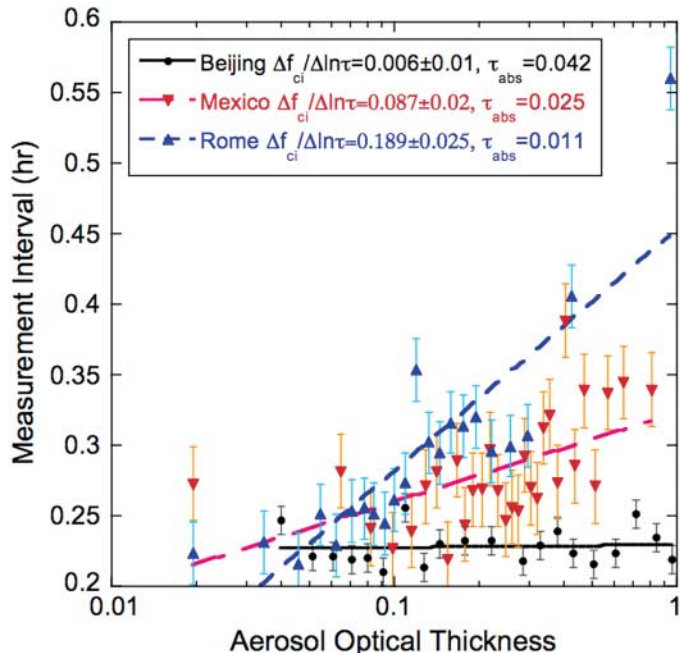


Fig. 1. Global distribution of the AERONET sunphotometers used in the analysis. The background is the average τ (a measure of the aerosol column concentration) for the year 2004 measured by MODIS on the Terra satellite. Green stars, continental sites in North America, Europe, and Asia; blue stars, marine locations in North America, the Mediterranean region, and Asia; red stars, biomass-burning sites in Africa and South America.

Fig. 2. Scatterplots of the time interval between two adjacent AERONET aerosol measurements that were not obscured by clouds, as a function of the average τ around the interval. The three examples are for low τ_{abs} (blue line and triangles; Rome, Italy from September to October; $\tau_{abs} = 0.011$), medium τ_{abs} (red line and triangles; Mexico City, Mexico from July to August; $\tau_{abs} = 0.025$), and high τ_{abs} (black line and circles; Beijing, China from September to October; $\tau_{abs} = 0.042$). Four years of data were used for each site for the 2 calendar months. The data were sorted by τ and averaged in groups of 100. The error bars are the standard error for each point. The corresponding changes in the cloud cover, $\Delta f_{ci}/\Delta \ln\tau$, are shown.



representing the value of absorption that competes with the number of potential cloud condensation nuclei in determining the cloud fraction.

In order to study the effect of pollution and smoke aerosols, we restricted the data to locations and periods with minimal dust influence. To have enough points for each time increment, we also restricted the data to cloud systems that passed over the site during no more than 3 hours (27). As a result, the observations were weighted toward meteorological systems with broken clouds.

The results for the change in cloud cover Δf_{ci} with a change in $\Delta \ln \tau$ are shown in Fig. 3 (see also table S1). Every point represents an analysis of ~ 3000 measurements. A linear fit to all of the data shows that

$$\frac{\Delta f_{ci}}{\Delta \ln \tau} = (0.17 \pm 0.01) - (3.5 \pm 0.5)\tau_{abs} \quad (5)$$

with a correlation of $r = 0.69$.

Uncertainties are represented by the standard errors in the average values, and the 95% confidence level range of the slopes is between -2.6 and -4.4 . There is a smooth transition from aerosol enhancement of cloud cover to aerosol decrease of the cloud cover (Fig. 3).

Does Eq. 5 represent the aerosol effect on cloud cover, cloud processing of aerosols, or coincidental variations of clouds and aerosol with the meteorological field? To address this question, we subdivided the data in Fig. 3A into three geographical regions (colored stars in Fig. 1): continental Northern Hemisphere sites with pollution aerosols, coastal marine sites, and biomass-burning sites in Africa and South America (25, 26, 28). These regions differ in aerosol and cloud properties; however, the slope of $\Delta f_{ci}/\Delta \ln \tau$ versus τ_{abs} for these regions varies within the uncertainty range of Eq. 5.

The fact that we have the same relationship for smoke and pollution aerosol is of special importance. Pollution aerosol is strongly hygroscopic, and thus variation in the humidity from 0% to 85% can triple the value of τ (29). Smoke is much less hygroscopic; an increase in the humidity to 85% increases τ by only 20% (30). The similarity in the regressions shows that it is unlikely that aerosol humidification in conditions that favor cloud formation is responsible for the increase of cloud cover with either an increase in aerosol concentration or its decrease with the introduction of τ_{abs} . The same can be said about cloud processing, which affects pollution aerosol

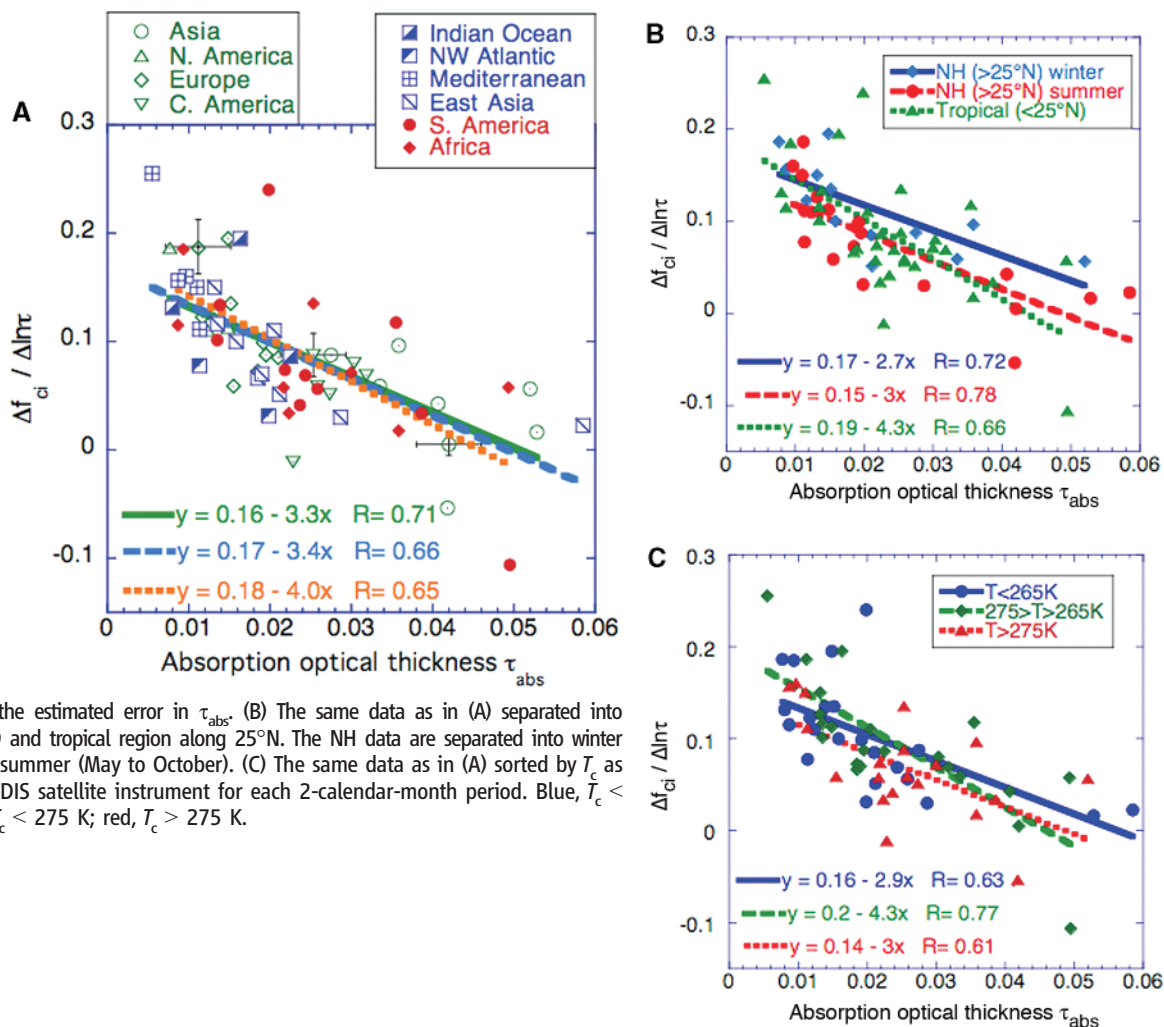
through sulfate production, which is not important for aerosols produced by biomass burning.

To address possible effects from seasonal variability, we subdivided the data in Fig. 3B based on season (winter to spring and summer to fall) in the Northern Hemisphere and year-long data in the Tropics. Alternatively in Fig. 3C, we separated the data by the cloud-top temperature (T_c) obtained from Moderate Resolution Imaging Spectroradiometer (MODIS) satellite data (31, 32). In all of these cases, the slopes of $\Delta f_{ci}/\Delta \ln \tau$ versus τ_{abs} varied within the uncertainty of Eq. 5.

To what degree can the relationship in Eq. 5 be influenced by atmospheric dynamics? Convergence zones and updrafts can increase the depth of the boundary layer, the column concentration of aerosols, and total precipitable water vapor. They can also promote cloud cover (33). Analysis of aerosol and water vapor separately for each location and season shows significant correlations between τ and the total precipitable water vapor (Fig. 3), which is a possible indication of the effect of convergence. The results, summarized in Table 1, show that $\sim 25\%$ of the relationship of Δf_{ci} with τ may be associated with variation of the precipitable water vapor. As expected, the effects are stronger for

Fig. 3. Regional (A), seasonal (B), and T_c (C) analyses of the AERONET data for the effect of aerosols on cloud cover. $\Delta f_{ci}/\Delta \ln \tau$ was plotted as a function of τ_{abs} . Each point represents an analysis of ~ 3000 measurements from a given location and 2 calendar months averaged over 3 to 5 years. (A) Green symbols indicate continental sites, blue symbols indicate marine sites, and red symbols indicate biomass-burning sites. For distribution of the sites, see Fig. 1. Error bars are printed for three representative points and indicate the average uncertainties in the least-squares fit used

for individual points and the estimated error in τ_{abs} . (B) The same data as in (A) separated into Northern Hemisphere (NH) and tropical region along 25°N . The NH data are separated into winter (November to April) and summer (May to October). (C) The same data as in (A) sorted by T_c as determined from the MODIS satellite instrument for each 2-calendar-month period. Blue, $T_c < 265$ K; green, $265 \text{ K} < T_c < 275$ K; red, $T_c > 275$ K.



pollution aerosol in the Northern Hemisphere than for biomass burning in the tropics, where the dry season is associated with smaller meteorological variability (34).

We found a consistent relationship between an increase in the cloud fraction and an increase in τ (representing column concentration), as well as a decrease in τ_{abs} . The relationship is invariant to the location or to the aerosol type. About 25% of the relationship of clouds to aerosol can be explained by the variation of total precipitable water vapor and may be associated with atmospheric convergence. What are the consequences of this systematic effect of aerosol on the cloud cover?

We used the limited global sample of aerosol interaction with clouds from Fig. 3 to roughly estimate the global average anthropogenic aerosol impact on cloud cover over the oceans. For a global average aerosol (excluding dust) single scattering albedo of 0.92 ± 0.05 (25, 26) and an average total optical depth value of $\tau = 0.093 \pm 0.02$ over the oceans [composed of $\tau = 0.06 \pm 0.01$ (for baseline natural aerosol) and $\tau = 0.033 \pm 0.01$ (for anthropogenic aerosols) (35, 36)], we obtained a τ_{abs} value of 0.007 ± 0.005 . From Table 1, we acquired a $\delta f_{\text{ci}}/\delta \ln \tau$ value of 0.11 ± 0.02 . Anthropogenic aerosol increases the fine τ over the oceans, which provide most of the cloud condensation nuclei, from baseline values of 0.03 ± 0.01 to 0.065 ± 0.02 (35, 36). For an average cloud cover of 0.6, the increase in τ corresponds to a change in cloud cover of

$$\begin{aligned} \Delta f_c &= \Delta f_{\text{ci}}(1 - f_c) = 0.11 \Delta \ln \tau (1 - 0.6) \\ &= 0.03 \pm 0.01 \end{aligned} \quad (6)$$

The spatial distributions of aerosol over the oceans and their absorption properties are highly heterogeneous. Consequently, the estimated average impact is uncertain and should be viewed as a first approximation. The clouds sampled by the AERONET procedure do not include extended cloud systems that are sensitive to aerosol effect. The analysis applies to urban industrial pollution and aerosol produced by biomass burning rather than land-use-generated dust.

The relationship between cloud cover and aerosol given by Eq. 5 can serve as a constraint on models of the aerosol and cloud interaction, independently of the cause-and-effect relationship. The robustness of the effect of aerosols on clouds, presented here, makes it more likely that most of the observed changes in the cloud cover are due to the aerosol impact. The large effect of elevated aerosol concentration on cloud cover, an increase of 0.03 (5%) in average cloud cover (Eq. 6), can have a profound effect on the hydrological cycle and climate.

References and Notes

- V. Ramanathan *et al.*, *Science* **294**, 2119 (2001).
- J. Haywood, O. Boucher, *Rev. Geophys.* **38**, 513 (2000).
- B. A. Albrecht, *Science* **245**, 1227 (1989).
- L. D. Rotstajn, Y. G. Liu, *Geophys. Res. Lett.* **32**, 10.1029/2004GL021922 (2005).
- R. Gunn, B. B. Phillips, *J. Meteorol.* **14**, 272 (1957).
- S. Menon *et al.*, *J. Atmos. Sci.* **59**, 692 (2002).
- K. M. Lau, M. K. Kim, K. M. Kim, *Clim. Dyn.* 10.1007/s00382-006-0114 (2006).
- D. Rosenfeld, *Science* **287**, 1793 (2000).
- M. O. Andreae *et al.*, *Science* **303**, 1337 (2004).
- A. S. Ackerman *et al.*, *Science* **288**, 1042 (2000).
- J. E. Penner *et al.*, *Climate Change 2001: The Scientific Basis*, J. T. Houghton *et al.*, Eds. (Cambridge Univ. Press, New York, 2001), pp. 289–348.
- Y. J. Kaufman, I. Koren, L. A. Remer, D. Rosenfeld, Y. Rudich, *Proc. Natl. Acad. Sci. U.S.A.* **102**, 11207 (2005).
- I. Koren, Y. J. Kaufman, L. A. Remer, D. Rosenfeld, Y. Rudich, *Geophys. Res. Lett.* **32**, 10.1029/2005GL023187 (2005).
- A. Devasthale, O. Kruger, H. Grassl, *IEEE J. Trans. Geosci. Remote Sens.* **2**, 333 (2005).
- I. Koren, Y. J. Kaufman, L. A. Remer, J. V. Martins, *Science* **303**, 1342 (2004).
- O. Kruger, H. Grassl, *Geophys. Res. Lett.* **31**, 10.1029/2001GL014081 (2004).
- G. Feingold, H. L. Jiang, J. Y. Harrington, *Geophys. Res. Lett.* **32**, 10.1029/2004GL021369 (2005).
- J. Hansen, M. Sato, R. Ruedy, *J. Geophys. Res.* **102**, 6831 (1997).
- M. Z. Jacobson, *J. Phys. Chem. A* **110**, 6860 (2006).
- M. Sekiguchi *et al.*, *J. Geophys. Res.* **108**, 10.1029/2002JD003359 (2003).
- J. Zhang, J. S. Reid, B. N. Holben, *Geophys. Res. Lett.* **32**, 10.1029/2005GL023254 (2005).
- B. N. Holben *et al.*, *Remote Sens. Environ.* **66**, 1 (1998).
- B. N. Holben *et al.*, *J. Geophys. Res.* **106**, 12067 (2001).
- Y. J. Kaufman, G. P. Gobbi, I. Koren, *Geophys. Res. Lett.* **33**, 10.1029/2005GL025478 (2006).
- O. Dubovik *et al.*, *J. Atmos. Sci.* **59**, 590 (2002).
- Y. J. Kaufman, O. Dubovik, A. Smirnov, B. N. Holben, *Geophys. Res. Lett.* **29**, 10.1029/2001GL014399 (2002).
- The locations were selected outside of the African dust range. We used only periods with average Ångström exponent $\text{Å} > 1$, $\tau > 0.10$, and at least 1000 points. These conditions also excluded Asian dust. The requirement of 1000 points ensured that, for the variation of $\ln \tau$ of 0.7 and
- the measured average standard deviation of Δf_{ci} of 0.6, we get uncertainty in variation of $\Delta f_{\text{ci}}/\Delta \ln \tau < 0.03$. Individual AERONET data points were selected for solar zenith angle $< 60^\circ$, $\tau < 1$, and measurement interval < 3 hours.
- L. A. Remer, Y. J. Kaufman, *Atmos. Phys. Chem.* **6**, 237 (2006).
- R. A. Kotchenruther, P. V. Hobbs, D. A. Hegg, *J. Geophys. Res.* **104**, 2239 (1999).
- Y. J. Kaufman *et al.*, *J. Geophys. Res.* **103**, 31,783 (1998).
- M. D. King, Y. J. Kaufman, P. Menzel, D. Tanré, *IEEE J. Trans. Geosci. Remote Sens.* **30**, 2 (1992).
- Giovanni MODIS Online Visualization and Analysis System (MOVAS) (<http://lake.nascom.nasa.gov/movas/>).
- M. D. Chou, P. K. Chan, M. H. Wang, *J. Atmos. Sci.* **59**, 748 (2002).
- Y. J. Kaufman, R. S. Fraser, *Science* **277**, 1636 (1997).
- Y. J. Kaufman, A. Smirnov, B. N. Holben, O. Dubovik, *Geophys. Res. Lett.* **28**, 3251 (2001).
- Y. J. Kaufman *et al.*, *Geophys. Res. Lett.* **32**, 10.1029/2005GL023125 (2005).
- We thank T. Eck, B. Holben, L. Remer, J. Lu, E. Wilcox, and many others, including anonymous reviewers, for comments on the work; the AERONET project for maintaining consistent high data quality and easy availability and use of the data worldwide; and the numerous AERONET site principal investigators for their efforts in establishing and maintaining the sites. I.K. is the incumbent of the Benjamin H. Swig and Jack D. Weiler Career Development Chair.

Supporting Online Material

www.sciencemag.org/cgi/content/full/1126232/DC1

Materials and Methods

Fig. S1

Table S1

14 February 2006; accepted 21 June 2006

Published online 13 July 2006;

10.1126/science.1126232

Include this information when citing this paper.

Crustal Dilatation Observed by GRACE After the 2004 Sumatra-Andaman Earthquake

Shin-Chan Han,^{1*} C. K. Shum,¹ Michael Bevis,¹ Chen Ji,² Chung-Yen Kuo¹

We report the detection of an earthquake by a space-based measurement. The Gravity Recovery and Climate Experiment (GRACE) satellites observed a ± 15 -microgalileo gravity change induced by the great December 2004 Sumatra-Andaman earthquake. Coseismic deformation produces sudden changes in the gravity field by vertical displacement of Earth's layered density structure and by changing the densities of the crust and mantle. GRACE's sensitivity to the long spatial wavelength of gravity changes resulted in roughly equal contributions of vertical displacement and dilatation effects in the gravity measurements. The GRACE observations provide evidence of crustal dilatation resulting from an undersea earthquake.

The devastating 26 December 2004 Sumatra-Andaman undersea earthquake, with a moment magnitude (M_w) between 9.1 and 9.3, ruptured more than 1000 km of a locked subduction interface near northern Sumatra, Nicobar, and the Andaman islands (*I*). Measurements from global seismic network and Global Positioning System (GPS) stations have been used to infer the coseismic slip history of this event (*I–A*). The earthquake permanently changed the mass distribution within Earth and has consequently perturbed the motion of Earth-orbiting

satellites by an amount that is measurable from the ranging instrument onboard the Gravity Recovery and Climate Experiment (GRACE) satellites (5). GRACE consists of two identical satellites co-orbiting at low altitude (~ 450 km), separated by

¹Geodetic Science, Department of Geological Sciences, Ohio State University, 275 Mendenhall Laboratory, 125 South Oval Mall, Columbus, OH 43210–1398, USA.

²Department of Earth Sciences, University of California at Santa Barbara, Santa Barbara, CA, USA.

*To whom correspondence should be addressed. E-mail: han.104@osu.edu